Journal of Fluorine Chemistry 131 (2010) 898–906

Contents lists available at ScienceDirect

Journal of Fluorine Chemistry

journal homepage: www.elsevier.com/locate/fluor

Alkali metal cation complexation and solvent interactions by robust chromium(III) fluoride complexes

Torben Birk, Magnus J. Magnussen, Stergios Piligkos, Högni Weihe, Anders Holten, Jesper Bendix *

Department of Chemistry, University of Copenhagen, Universitetsparken 5, DK-2100 Copenhagen, Denmark

ARTICLE INFO

Article history:
Received 27 February 2010
Received in revised form 7 June 2010
Accepted 8 June 2010
Available online 15 June 2010

Keywords:
Bridging
Cr(III)
Robust
Linear
Chain

ABSTRACT

Interaction of robust chromium(III) fluoride complexes with sodium or lithium cations in solution lead to hypsochromic spectral shifts of increasing magnitude along the series: *trans*-$[CrF_2(py)_4]^+$, *mer*-$[CrF_3(terpy)]$, and *fac*-$[CrF_3(Me_3tacn)]$. Crystalline products isolated from solution exhibit μ_2-bridging by the fluoride ligands in a linear fashion between Na^+-ions and chromium centres in *catena*-$[Na(H_2O)_4(\mu\text{-}F)\text{-}trans\text{-}\{CrF(py)_4\}](HCO_3)_2$ and in the dimers $[Li(H_2O)_n(\mu\text{-}F)\text{-}trans\text{-}\{CrF(py)_4\}]^{2+}$ ($n = 3, 4$). The uncharged chromium complexes *fac*-$[CrF_3(Me_3tacn)]$ and *mer*-$[CrF_3(terpy)]$ have been synthesized from *mer*-$[CrF_3(py)_3]$ and shown to precipitate sodium salts from solution, of which $3[CrF_3(Me_3tacn)]\cdot 2Na(Bph_4)\cdot solv$ and $6[CrF_3(terpy)]\cdot 4Na(Bph_4)\cdot solv$ have been crystallographically characterized. In these clusters, the neutral fluoride complexes bring the Na^+ cation separation down to 3.610 Å and 3.369 Å, respectively, which is much closer than the inter-cation distance in NaCl and comparable to that of NaF. DFT calculations support the notion of a strong interaction between Na^+ ions and neutral chromium(III) fluoride complexes. The calculations reproduce the magnitude and the counter-intuitive sign of the spectral shifts induced by second sphere complexation in solution, which originates in a breakdown of the assumption of parameter transferability in ligand-field descriptions.

1. Introduction

The high propensity of fluoride for hydrogen bonding [1–4] and interactions with hard (or type-A) cations [5–9] makes fluoride complexes candidates for investigation of second sphere coordination as well as possible structure-directing building blocks in the synthesis of framework structures. Interaction of fluoride complexes with protic solvents leading to solvatochromism is well established and has been investigated especially by Kaizaki and co-workers [10–13]. However, spectral consequences of more general second sphere interactions have not been reported for fluoride complexes and the possibility of spectroscopic cation sensing by fluoride complexes has not been investigated. Also in the solid state, fluoride is known to bridge between metal ions in molecular entities in a multitude of ways: linear μ_2 [14], bent μ_2 [15], symmetrical μ_3 [16], unsymmetrical μ_3 [17], μ_4 [18], and μ_6 [19], but with a quite distinct preference for (almost) linear μ_2-bridging.

Here, we show that robust chromium(III)fluoride complexes interact not only with protic solvents, but also with alkali metal ions in solution. The second sphere coordination results in clustering or chain formation in the solid state where novel types of fluoride-bridged heterometallic dimers (Li^+) or chain polymers (Na^+) can be isolated starting from the *trans*-$[CrF_2(py)_4]^+$ cation. The ability of fluoride to tightly assemble cations is further demonstrated by co-crystallization of the uncharged chromium complexes *fac*-$[CrF_3(Me_3tacn)]$ and *mer*-$[CrF_3(terpy)]$ with sodium tetraphenylborate leading to sodium cation clustering with notably short separations between the sodium cations. The apparent, counter-intuitive increase in donor strength of fluoride upon second sphere complexation is studied by DFT calculations, which show ligand synergies and thus illuminate the problems associated with ligand-field descriptions of the phenomenon.

2. Results and discussion

2.1. Syntheses

Direct reaction between *trans*-$[CrF_2(py)_4]^+$ and lithium or sodium salts in water yields crystalline products containing partially solvated alkali metal ions which also coordinate fluoride(s) from the chromium complex. It is noteworthy, that even a cationic fluoride complex competes efficiently with water as ligand for the Li^+ and Na^+ ions. The specific salts in consideration here were selected as some of those yielding crystalline products among a range of attempted reactions all executed under similar

* Corresponding author. Tel.: +45 35320101.
E-mail address: bendix@kiku.dk (J. Bendix).

0022-1139/$ – see front matter © 2010 Elsevier B.V. All rights reserved.
doi:10.1016/j.jfluchem.2010.06.003

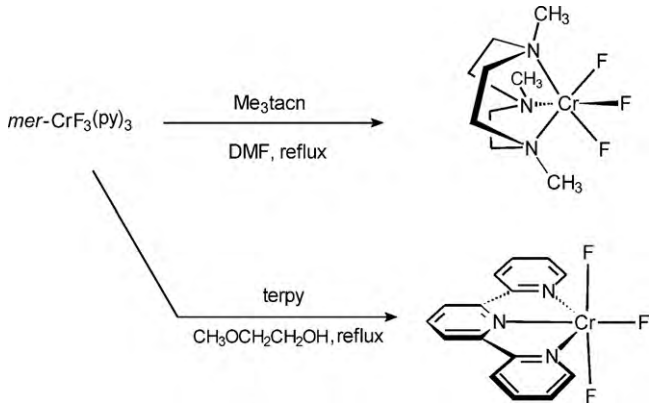

Scheme 1. Synthesis of facial and meridional neutral chromium(III) fluoride complexes.

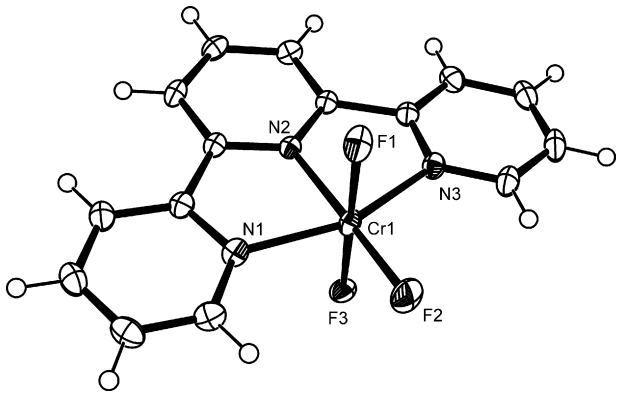

Fig. 1. Molecular structure of $[CrF_3(terpy)]$ in **3**. Bond lengths (Å) around the chromium(III) centre: Cr–F1 1.9033(16), Cr–F2 1.8671(16), Cr–F3 1.8915(16), Cr–N1 2.080(2) Cr–N2 2.009(2), Cr–N3 2.078(2). Bond angles (°): F2–Cr1–F3 92.48(8), F2–Cr1–F1 89.93(8), F3–Cr1–F1, 177.10(7); N2–Cr1–N3, 78.19(8); N2–Cr1–N1, 78.14(8).

conditions. The use of chromium fluoride complexes as ligands for hard cations is of wide scope, but naturally limited by interactions between counter ions from the chromium complex and the targeted hard metal ions. Thus, fluoride complexes with weakly coordinating counter ions or ideal complexes without counter ions altogether are preferable. To realize the latter situation we targeted neutral chromium(III) fluoride complexes, which at the same time are as robust as possible by using tridentate auxiliary ligands. The two possible configurations *fac* and *mer* were imposed on the chromium centre by the use of the geometrically constrained ligands 1,4,7-trimethyl-1,4,7-triazacyclononane (Me_3tacn) and 2,2′;6′,2″-terpyridine (terpy), respectively. The two new complexes were synthesized as outlined in Scheme 1 from the same starting material employing reflux in a solvent with a higher boiling point than the expelled pyridine.

The uncharged complexes were found to precipitate sodium salts such as NaI or $Na(Bph_4)$ efficiently from weak donor solvents. Again the reaction is of wide scope, complicated mainly by the need for carefully chosen conditions to obtain well-crystallized products. In general, the fluoride complexes are poorly soluble in non-protic solvents while in most cases, though not for the tetraphenylborate salts, water competes too well and prevents the isolation of fluoride-bridged compounds. Accordingly, alcohols were found suitable for the isolation of polynuclear M^I–F–Cr^{III} systems.

2.2. X-ray crystallography

2.2.1. Coordination geometry and bonding

In $[CrF_3(terpy)]\cdot 2.5H_2O$ (**3**) the chromium centre is coordinated with a distorted octahedral environment with meridional geometry imposed by the terpyridine ligand. The complex is shown in Fig. 1 and relevant metric data are given in the figure caption.

There are no other structurally characterized, monomeric, uncharged six-coordinate chromium(III) complexes with terminal fluoride ligands. Chromium fluoride bond lengths are slightly longer than those found for structurally characterized cationic, cis-$[Cr(phen)_2F_2](ClO_4)\cdot H_2O$ with Cr–F at 1.844 Å and 1.862 Å [20] and (1.857 Å) in *trans*-$[CrF_2(py)_4](PF_6)$ [21], but close to the Cr–F distances in anionic $[CrF_4(py)_2]^-$ (1.881 Å; 1.893 Å) [22]. The chromium nitrogen bond distances are close to those found in $[CrCl_3(terpy)]\cdot$dmso (1.992 Å, 2.071 Å, 2.078 Å) [23].

The double salt *trans*-$[CrF_2(py)_4][Cr(py)_4F(\mu\text{-}F)Li(H_2O)_3][Cr(py)_4F(\mu\text{-}F)Li(H_2O)_4]Cl_5\cdot 6H_2O$ (**1**) contains, in addition to the parent cation *trans*-$[CrF_2(py)_4]^+$, two different dimeric, fluoride-bridged complexes, with 4 and 5 coordinate lithium ions, respectively. The structures are depicted in Fig. 2 with bond lengths given in the figure text.

The fluoride bridges in the Li–F–Cr dimers are almost linear at 164° and 171° and there is very little (0.00–0.02 Å) elongation of the Cr–F bonds upon coordination to the lithium cation. In the

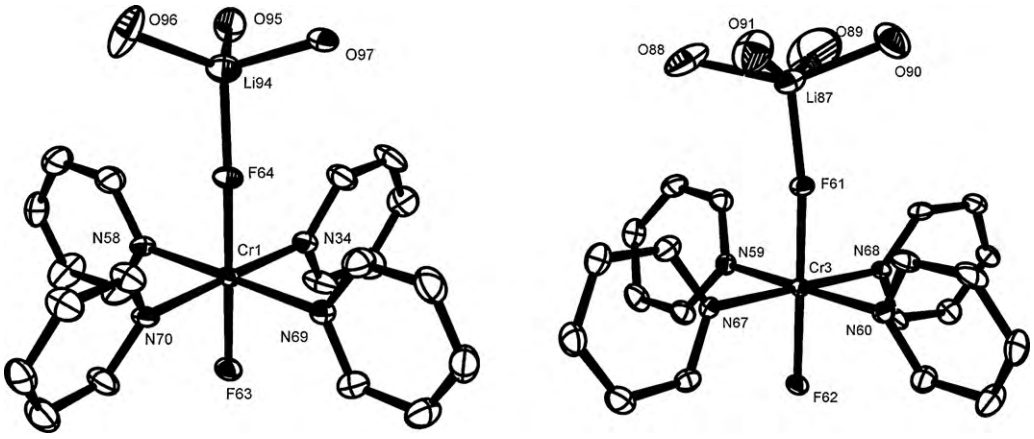

Fig. 2. Ortep drawings of the two heterometallic dimers in **1**, illustrating **4** and **5** coordinate Li^+ cations in *trans*-$[Cr(py)_4F(\mu\text{-}F)Li(H_2O)_3]^{2+}$ and *trans*-$[Cr(py)_4F(\mu\text{-}F)Li(H_2O)_4]^{2+}$, respectively. Hydrogen atoms are omitted for clarity. Selected bond lengths (Å): Cr1–N(av) 2.086(3), Cr1–F63 1.852(2), Cr1–F64 1.8754(19), Li94–F64 1.862(6), Li94–O95 1.934(6), Li94–O96 1.887(6), Li94–O97 1.905(6), Cr3–N(av) 2.083(2), Cr3–F61 1.8699(19), Cr3–F62 1.8623(19), Li87–F61 1.874(6), O89–Li87 2.176(9), O88–Li87 2.016(7), O90–Li87 1.930(7), O91–Li87 2.037(8). Selected bond angles (°): Li94–F64–Cr1 164.12(19), Cr3 F61 Li87 170.7(2).

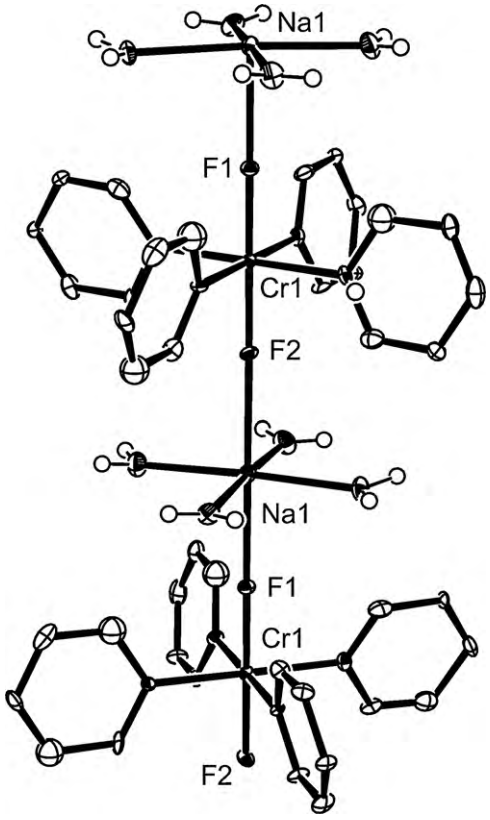

Fig. 3. Part of the chain in **2**, encompassing more than one asymmetric unit. All metal atoms lie on fourfold axes. Hydrogen atoms on the pyridine ligands are omitted for clarity. Selected bond lengths (Å): Cr1–F1 1.8750(8), Cr1–F2 1.8635(7), Cr1–N 2.0834(5), Na1–F1 2.4904(9), Na1–F2 2.4066(9), Na1–O 2.3516(6). Selected bond angles (°): F1–Cr1–F2 180, F2–Cr1–N1 89.779(13), F1–Cr1–N1 90.221(13).

coordination spheres of the Li^+ ions, the average bond lengths to the water ligands depend quite strongly (>0.1 Å) on the coordination number of the Li^+, whereas the Li–F distance (1.862(6) Å and 1.874(6) Å, respectively) is independent of the number of water ligands. Notably, both Li–F bonds in this double salt are shorter than the lithium–water bonds. The fact that the fluoride ion is part of a very weakly structurally perturbed, cationic complex makes this an unexpected observation and demonstrates a quite pronounced donor functionality of the coordinated fluoride towards hard metal ions.

In *catena*-$[Na(H_2O)_4][Cr(py)_4F_2](HCO_3)_2$ (**2**), the tendency towards linear fluoride bridges results in an unprecedented one-dimensional chain polymer containing linear fluoride bridges to the sodium cations. Other examples of linear fluoride bridging among transition metals only include $[pyH]_2[Cu(py)_4(MX_6)_2]$ ($MX_6 = ZrF_6^{2-}$, $NbOF_5^{2-}$, $MoO_2F_4^{2-}$; py = pyridine) [24a] and *catena*-(bis(μ_2-fluoro)-bis(μ_2-oxo)-octafluoro-octakis(pyridine)-di-cadmium-di-niobium) [24b]. In Fig. 3 the structure of the chain without the counter ions is depicted.

As for the structure of **1** described above, the chromium coordination sphere is only slightly perturbed with Cr–F bond length elongations <0.02 Å upon Na^+ complexation. Cr–N bond lengths vary only little and their average is identical to that found in the two lithium cation complexed dimers in **1**. The octahedral *trans* configuration around the sodium cations is elongated along the chain axis with Na–F on average being 0.1 Å longer than the Na–O bonds. The water molecules coordinated to the sodium cations are coordinated in a planar (sp^2-hybrized) fashion with the planes of all four water molecules perpendicular to the chain direction. Normally, this coordination mode is found only when the metal is a good π-acceptor, which obviously is not the case here, where this geometry is imposed by hydrogen bonding to the hydrogen carbonate counter ions (*vide supra*).

Precipitation of $[CrF_3(terpy)]$ (**3**) with $NaBph_4$ in methanol yields the decanuclear cluster shown in Fig. 4.

The cluster contains six uncharged chromium complexes and four sodium cations. Surrounding the cluster, but not shown in the figure are four essentially non-interacting Bph_4^- counter ions. The most prominent feature of the structure is the very short Na^+–Na^+ contacts (3.369 Å and 3.550 Å), which means that the bridging chromium complexes bring the Na^+ ions significantly closer than in NaCl (3.98 Å). As the cluster is situated at a centre of inversion there are only two distinct environments for the Na^+ ions in the structure. The terminal Na^+ ions are five coordinate in a distorted trigonal bipyramid geometry with three fluoride and two methanol (equatorial) ligands. Fluoride bond lengths to the terminal Na^+ ions vary from 2.202 Å to 2.312 Å and sodium–oxygen distances are 2.285 Å and 2.329 Å. The middle Na^+ ions are coordinated by six fluorides in a very irregular geometry with large variation also in bond lengths with Na–F ranging from 2.199 Å to 2.590 Å. The strong interaction between the Na^+ ions and the chromium complexes is also evident from very short Na–Cr distances of 3.248–3.419 Å. Within each cluster the terpyridine ligands are arranged in three distinct layers (Fig. 4, top). With inter-layer distances of 3.5–4.0 Å, π-stacking may stabilize this arrangement, but most likely the rigidity of the chromium complexes in combination with electrostatic repulsion between Na^+ ions determine the structure. As for the structures involving *trans*-$[CrF_2(py)_4]^+$, the Cr–F distances in the terpyridine complexes are at 1.851–1.919 Å only little perturbed by coordination to the Na^+ ions. Actually, Cr–F distances in **4** are on average (1.882 Å) slightly shorter than in the parent chromium complex, **3** (1.887 Å).

With the facial fluoride complex $[CrF_3(Me_3tacn)]$ (**5**), the pentameric cluster in Fig. 5 results.

Also in this cluster, the Na^+ ions are tightly bound with a Na^+–Na^+ distance of 3.61 Å. In **6**, both Na^+ ions are six-coordinated with distorted octahedral geometries. One (Na99) is coordinated by four fluorides, a water molecule and a 2-propanol molecule; the other (Na100) by five fluorides and one water molecule. For both sodium centres, one of the Na–F interactions is very long: 2.857(2) Å for Na99 and 2.989(2) Å for Na100, while the other distances are similar to those found in **4**: 2.194–2.391 Å at Na99 and 2.229–2.335 Å at Na100. The central fluoride (F10) is coordinated in an almost planar T-shaped geometry, bridging Cr3 and Na100 by an angle of 159.7°. As in **4** the tight bonding of the sodium cations also in **5** results in short Cr–Na distances (3.238–3.481 Å).

2.2.2. Crystal packing

Hydrogen bonding assembles the dimers containing four and five coordinate lithium cations into two distinct, parallel chains along the crystallographic *b*-axis. The hydrogen bonds of both chains connect one of the water ligands to Li^+ with the distant terminal fluoride at the chromium centre of the respective dimers (cf. Fig. 6).

All ligating water molecules in **1** are coordinated in a planar fashion with all water ligands on the five coordinate lithium centres oriented parallel to the dimer axis and the chain axis. At the four-coordinate lithium centres two of the water molecules are oriented perpendicular to the dimer axis and only the one engaged in the hydrogen bonds along the chain has its plane parallel to the Li–F–Cr axis. The hydrogen bonds are moderately strong gauged by their lengths (2.681 Å; 2.751 Å) and illustrate again that the donor character of fluoride by no means are quenched by coordination to a trivalent chromium centre, not even when the resulting complex is cationic. This situation differs

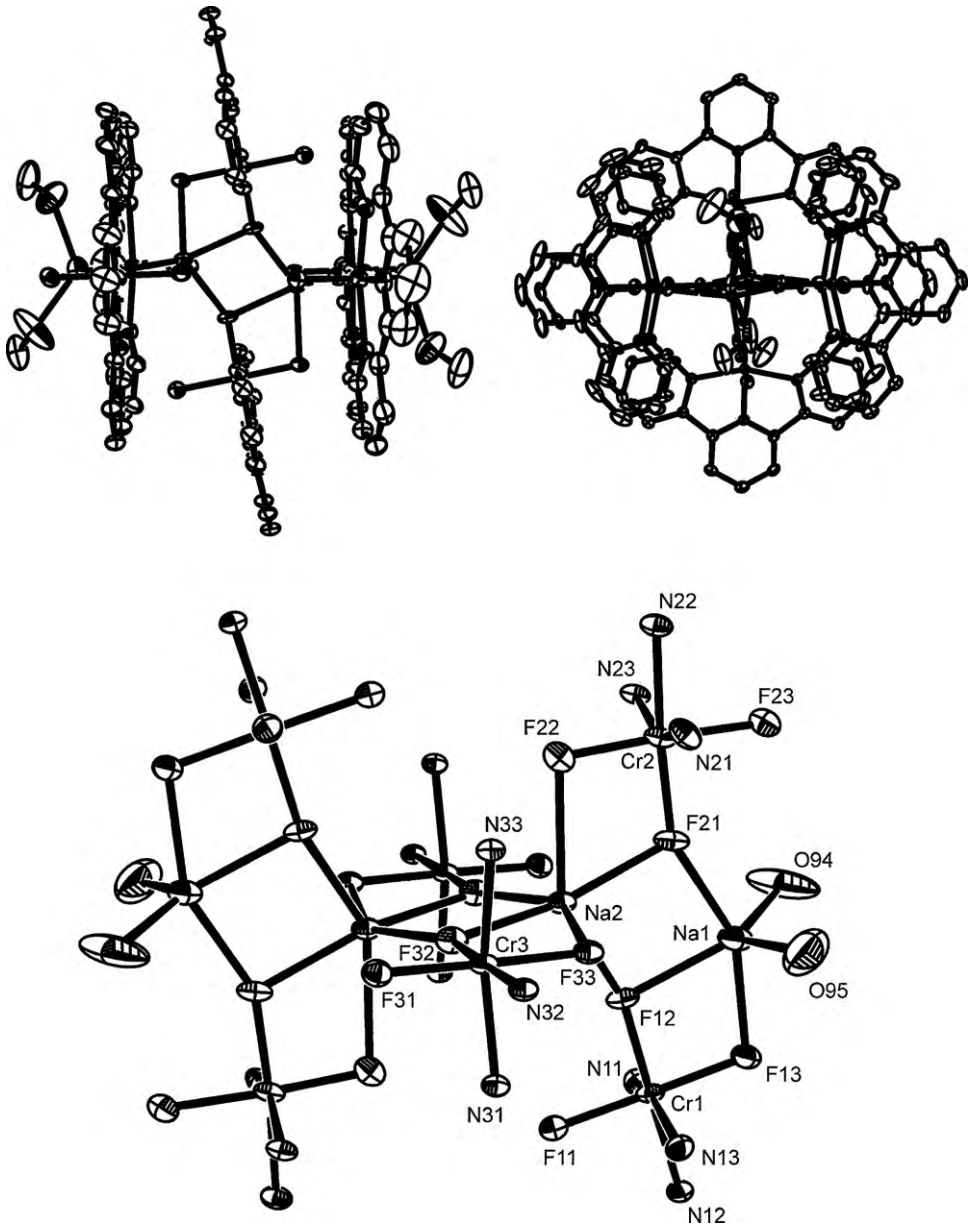

Fig. 4. Three orthogonal views of the cationic cluster $\{6[CrF_3(terpy)]\cdot 4Na\ 4MeOH\}^{4+}$ in **4**. Hydrogen atoms are omitted for clarity in the two top views. In the bottom view all atoms except the metal centres and the directly ligating atom are omitted. The cluster is situated at an inversion centre in the structure. Selected bond lengths (Å): Cr1–F(av) 1.882, Cr2–F(av) 1.884, Cr3–F(av) 1.881, F12–Na2 2.273(3), F1–Na1 2.312(3), F13–Na1 2.258(3), F21–Na1 2.202(3), F21–Na2 2.300(3), F22–Na2 2.589(3), F32–Na2 2.199(3), F33–Na2 2.398(3), Na1–O94 2.285(6), Na1–O95 2.328(6). Selected bond angles (°): O94–Na1–F12 127.3(3), O94–Na1–O95 121.6(3), F12–Na1–O95 110.9(2).

from the tendency of oxygen as a donor which differs markedly between cationic *trans*-$[M(O)F(dppe)_2]^+$ and neutral *trans*-$[M(O)_2(dppe)_2]$ [25].

In **1**, the Li^+ ions show no interaction with the chloride counter ions; the latter participating instead in a hydrogen bond pattern illustrated in Fig. 7.

In **2**, the linear Cr–F–Na–F–Cr... chains are held together by a layer structure in the perpendicular directions. All sodium cations are thus equatorially coordinated by four planar ligating water molecules which each hydrogen bond to two different hydrogencarbonate dimers (cf. Fig. 8). Each hydrogencarbonate dimer is held together by moderately strong hydrogen bonds with lengths at 2.621 Å. The hydrogen bonds between the water molecules ligating the sodium cation and the counter ions are longer at 2.830–2.914 Å, but almost linear (167.14°, 176.06°) and thus also to be classified as moderately strong.

2.3. Spectroscopic characterization

Solvatochromism of chromium(III) fluoride complexes is well established and attributed to solvent interactions with coordinated fluoride. In order to gauge whether the second sphere interaction demonstrated in the solid state structures persist in solution, the influence of Li^+ and Na^+ ions, as well as that of the solvent was examined for the absorption spectra of *trans*-$[CrF_2(py)_4]^+$, *mer*-$[CrF_3(terpy)]$ (**3**), and *fac*-$[CrF_3(Me_3tacn)]$ (**5**). The spectrum of *trans*-$[CrF_2(py)_4]^+$ is only very weakly solvent dependent and even high concentrations (1 M) of Li^+ produce only marginal shifts (ca. 2 nm; $<100\ cm^{-1}$) of the first spin-allowed transition, which for d^3-systems directly measure the octahedral component (Δ_O) of the ligand-field. The spectra of the trifluoro complexes are significantly more sensitive towards the solvent as well as towards Li^+ and Na^+ ions in solution. Data are shown in Fig. 9.

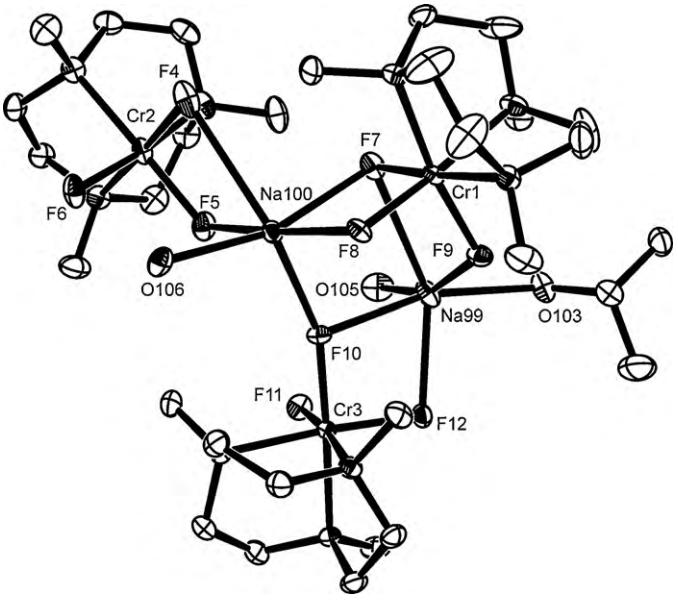

Fig. 5. Structure of the metal ion cluster in **6**. All hydrogen atoms including those of the water molecule are omitted for clarity. Selected bond lengths (Å): Cr1–F(av) 1.8779, Cr2–F(av) 1.8750, Cr3–F(av) 1.8904, Na99–F7 2.857(2), Na99–F9 2.194(2), Na99–F10 2.391(2), Na99–F12 2.341(2), Na99–O105 2.359(3), Na99–O103 2.390(2), Na100–F4 2.989(2), Na100–F5 2.229(2), Na100–F7 2.329(2), Na100–F8 2.3348(19), Na100–F10 2.2680(19), Na100–O106 2.373(2). Selected bond angles (°): Cr3–F10–Na100 159.70(9), Cr3–F10–Na99 98.75(8), Na100–F10–Na99 101.55(7), Cr1–F9–Na99 114.41(9), Cr1–F7–Na100 99.82(8), Cr1–F7–Na99 89.81(7), Na100–F7–Na99 87.62(6), Cr1–F8–Na100 99.78(8), Cr3–F12–Na99 100.17(8), Cr2–F5–Na100 115.91(9), Cr2–F4–Na100 88.19(8).

It is seen that for *mer*-[CrF_3(terpy)] (**3**), going from 2-propanol to water produces a hypsochromic shift of the $^4A_2(O) \rightarrow {}^4T_2(O)$ transition of 25 nm (ca. 800 cm^{-1}), while Li^+ ions (0.25 M) shift the absorption by only 8 nm. Most sensitive is the facial complex, [CrF_3(Me_3tacn)] (**5**), where the spectral shift of the first spin-allowed absorption band between water and acetonitrile is 34 nm (1050 cm^{-1}), turning the blue acetonitrile solution pink–red upon addition of water. Staying in one solvent, 2-propanol, addition of Na^+ ions to a concentration of 0.5 M, produces a shift half as large (600 cm^{-1}) as that observed between water and acetonitrile. The second spin-allowed transition (at ca. 400 nm) and the spin-forbidden $^4A_2(O) \rightarrow {}^2E(O)$ transition (at ca. 700 nm), which is observed for the trifluoride complexes are both less sensitive to solvent/cation perturbation. In all cases increasing hydrogen bond propensity and second sphere coordination by metal ions produce shifts of the first band towards shorter wavelengths. This is unexpected if only the metal fluoride interaction is considered, since both effects would be expected to decrease the donor strength of the fluoride. It has been argued that the spectrochemical parameter Δ_O is encompassing both σ- and π-antibonding effects through the relation $\Delta_O = 3e_\sigma - 4e_\pi$ and that the increase in Δ_O can reflect a simultaneous decrease in σ- and π-perturbation with the latter decreasing most. An independent test of this interpretation can be provided by DFT which allows for independent study of the effects of the solvent and the second sphere complexation.

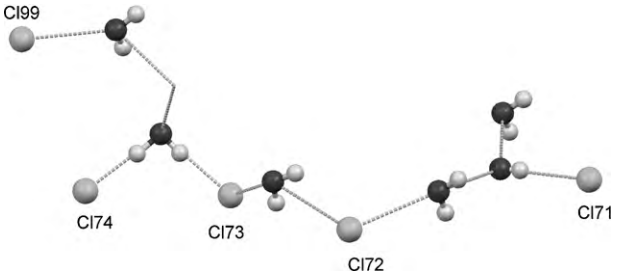

Fig. 7. Chloride-water packing in **1**.

2.4. DFT calculations

Mer-[$CrF_3(NH_3)_3$] and *fac*-[$CrF_3(NH_3)_3$] were chosen as computational models for *mer*-[CrF_3(terpy)] and *fac*-[CrF_3(Me_3tacn)] which are the systems exhibiting the largest spectral sensitivity towards solvent and alkali metal cation perturbations. Geometries of the two model systems were optimized computationally without any symmetry constraints in vaccum as well as in water modeled as a continuum (COSMO) [26]. In addition the geometry of the putative adduct {Na•*fac*-[$CrF_3(NH_3)_3$]}$^+$ was optimized in vacuum as well as solvated. The optimized structure of the adduct has the chromium complex functioning as a symmetrically coordinating η^3-ligand towards the Na^+ ion (Fig. 10).

While this structure is intuitively satisfying based on electrostatics it should be noted that this coordination mode with three μ_2-fluoride bridges has never been observed in heterobimetallic systems, the only known examples are a few $[M_2F_9]^{n-}$ ions. [27] Data for the optimized structures are collected in Table 1.

The thermodynamics of the adduct formation between *fac*-[$CrF_3(NH_3)_3$] and Na^+ was found to be strongly dependent on solvation. Calculations yielded a bonding energy of 269 kJ/mol in vacuum which was reduced to 80 kJ/mol when solvation (water, COSMO) was included.

The optimized structures show some general variations: solvation makes the structure more regularly octahedral for the facial as well as the meridional isomer; solvation and complexation with Na^+ has similar effects on the structure of *fac*-[$CrF_3(NH_3)_3$]; solvation results in longer Cr–F bonds and significantly shorter Cr–N bonds in all cases. The more regular structures obtained with solvation are expected based on dielectric shielding and concomi-

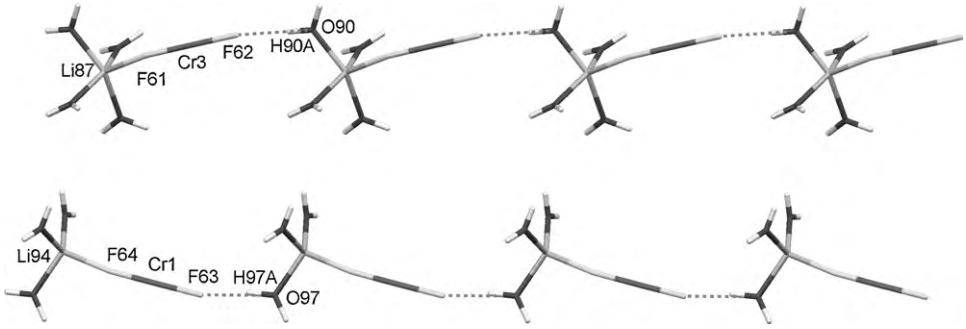

Fig. 6. Hydrogen bonding linking the dimeric units in **1** into parallel chains. Pyridine ligands on chromium as well as counter ions and non-bonded water molecules are omitted for clarity. Hydrogen bond lengths (Å): F62–O97 2.681, F62–O90 2.751.

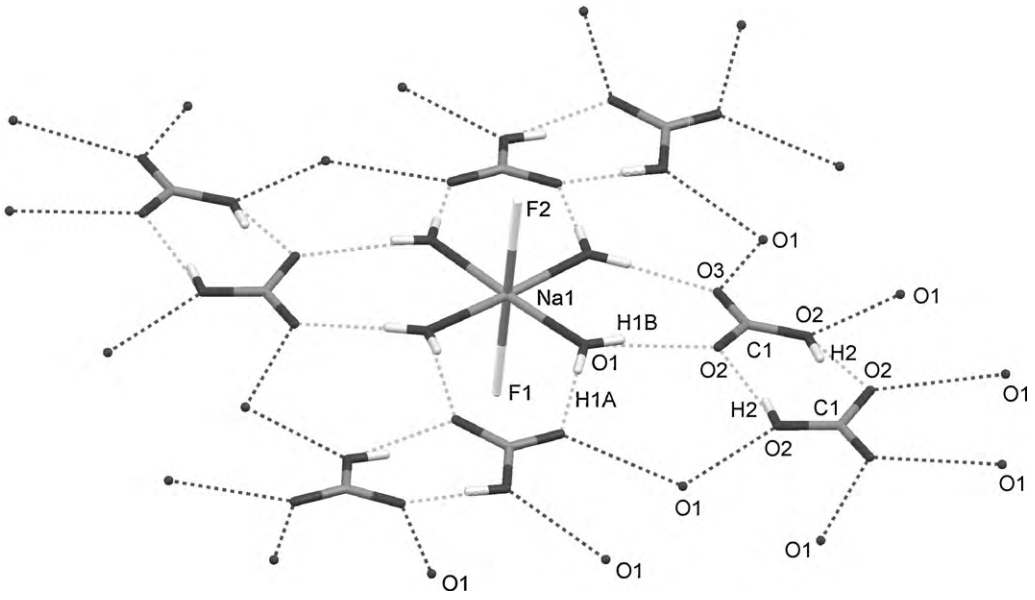

Fig. 8. Packing of the sodium-hydrogencarbonate layers in **2**. Only half of the 50% populated hydrogen positions in the hydrogencarbonate dimers are shown in order to reflect the compound composition. Hydrogen bond lengths (Å): O2–O2 2.621, O1–O2 2.914, O1–O3 2.830.

tant lower repulsion between the fluoride ligands. The similar response of the Cr–F bond length in the *fac*-isomer towards solvation and complexation is also expected since both phenomena results in less ionic contribution to the Cr–F bond. However, the pronounced contraction of the Cr–N bond lengths in *fac*-$[CrF_3(NH_3)_3]$ upon either solvation or complexation was not to be expected and demonstrates an inverse ligand–metal bond length correlation between the two types of ligands, which has the potential to invalidate the common assumption of transferability of ligand-field parameters between related complexes. Actually, the calculated Cr–N bond length contraction of 1.5–2.5% upon solvation (complexation) would lead to an increase of e_σ^N of ca. 10% (assuming $\Delta_O \propto r^{-5}$) or ca 2000 cm^{-1}, which is close in magnitude to the observed shifts.

Direct calculation of the solvent dependence of the spectra was attempted. TDDFT yields a poor reproduction of data producing a position of the first spin-allowed band which is 5000–7000 cm^{-1} too high in energy. The spectral shift upon going from vacuum to water is calculated ca. three times too large with the correct sign for the meridional complex, but with the wrong sign for the facial complex. It is, however, well known that TDDFT has pronounced shortcomings in reproducing positions of *d*–*d* transitions [28]. The

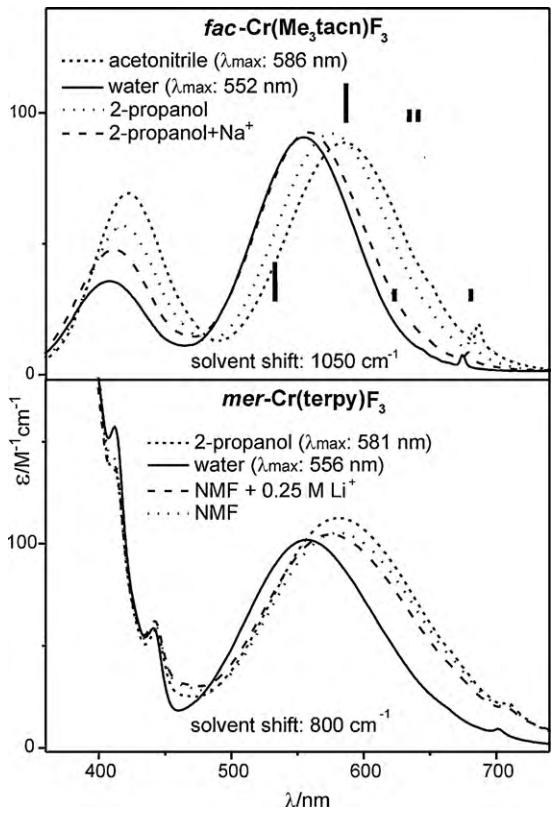

Fig. 9. Absorption spectra of *fac*-$[CrF_3(Me_3tacn)]$ (top) and *mer*-$[CrF_3(terpy)]$ (bottom) in various solvents and with addition of cations. The listed solvent shifts are maximal differences in the position of the $^4A_2(O) \rightarrow {}^4T_2(O)$ transition. In the top figure, the calculated band positions (SLT, *vide supra*) are shown by vertical lines. The upper lines are without and the lower ones with solvation (water, COSMO).

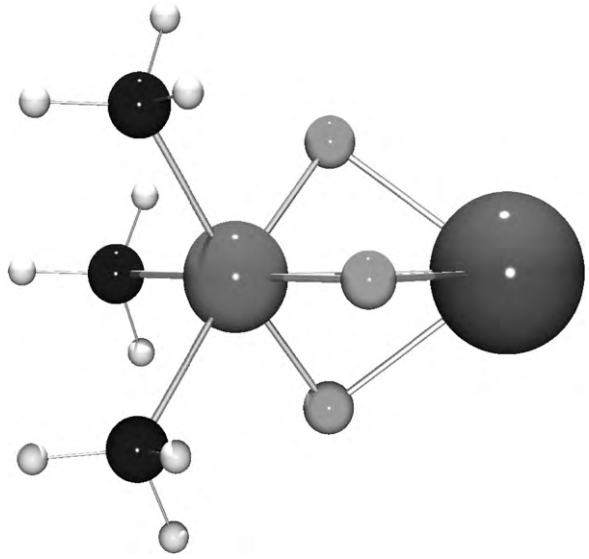

Fig. 10. DFT-optimized geometry for the adduct $\{Na\bullet$*fac*-$[CrF_3(NH_3)_3]\}^+$ in solution. No symmetry constraints were imposed on the optimization.

Table 1
DFT-optimized geometries for *mer*-[$CrF_3(NH_3)_3$], *fac*-[$CrF_3(NH_3)_3$] and {Na•*fac*-[$CrF_3(NH_3)_3$]}$^+$.

	mer-[$CrF_3(NH_3)_3$]		*fac*-[$CrF_3(NH_3)_3$]		{Na•*fac*-[$CrF_3(NH_3)_3$]}$^+$	
	Vacuum	Water (COSMO)	Vacuum	Water (COSMO)	Vacuum	Water (COSMO)
$(Cr–F)_{av.}$	1.873 Å	1.904 Å	1.860 Å	1.899 Å	1.877 Å	1.910 Å
$(Cr–N)_{av.}$	2.133 Å	2.106 Å	2.172 Å	2.114 Å	2.124 Å	2.094 Å
$(Na–F)_{av.}$	–	–	–	–	2.325 Å	2.308 Å
$(F–Cr–F)^{cis}_{av.}$	95.8°	91.6°	99.1°	92.7°	89.5°	88.0°
$(N–Cr–N)^{cis}_{av.}$	96.0°	90.6°	97.3°	90.6°	96.5°	91.9°

Slater Transition State method (SLT) has, on the other hand, been remarkably successful in calculation of *d–d* spectra and it does reasonably well also in this case. Band positions are calculated ca. 1000 cm^{-1} too high in water and with solvent shifts of the right sign between vaccum and water. The shifts calculated are 2100 cm^{-1} and 2600 cm^{-1} for the *mer*- and *fac*-complexes, respectively. The overestimated magnitude of the solvent shifts together with the slightly high energy calculated for the $^4A_2(O) \rightarrow {}^4T_2(O)$ transition in water has the consequence that the calculations in vacuum actually yield the experimental band positions in the lower polarity solvents very well. Data for the SLT calculations with and without solvation for the first spin-allowed and the first two spin-forbidden transitions are included as vertical lines in Fig. 9.

3. Experimental

3.1. Materials

The chromium complexes *trans*-[$CrF_2(py)_4$](NO_3) [29], $CrF_3(py)_3$ [30] and the ligand Me_3tacn [31] were synthesized according to the literature methods. terpy, LiCl (Aldrich) and $Na(Bph_4)$ (Merck) were obtained commercially and used as received. All solvents were used as received.

3.2. Syntheses

3.2.1. *trans-[$CrF_2(py)_4$][$Cr(py)_4F(\mu$-$F)Li(H_2O)_3$][$Cr(py)_4F(\mu$-$F)Li(H_2O)_4$]$Cl_5 \cdot 6H_2O$ (1)*

trans-[$CrF_2(py)_4$]NO_3 (10.071 g; 21.5 mmol) was dissolved in water (200 ml). The resulting violet solution was filtered through a wad of glass wool and solid LiCl (21.539 g; 0.508 mol) was added in batches of approximately 7 g, each batch being added only after the prior was completely dissolved. The solution was heated to 50 °C and subsequently cooled in an ice-water bath. After ca. 45 min crystallization of pink product commences. The product was isolated on a fritted filter funnel. Yield: 6.810 g (57.8% of theoretical based on chromium). Analysis: calcd. for $C_{60}H_{86}Li_2N_{12}O_{13}F_6Cl_5Cr_3$: H, 5.27%; C, 43.82%; N, 10.22%. Found: H, 5.04.%; C, 43.48%; N, 10.27%.

3.2.2. *catena-[$Na(H_2O)_4$][$Cr(py)_4F_2$](HCO_3)$_2$ (2)*

trans-[$CrF_2(py)_4$]NO_3 (10.031 g, 21.4 mmol) was dissolved in water (200 ml). The resulting violet solution was filtered through a wad of glass wool before heating up to 30 °C with stirring whereupon anhydrous $NaHCO_3$ (10.015 g, 119.2 mmol) was added. The addition of $NaHCO_3$ resulted in a cloudy reaction mixture and a change in color towards pink. Within a few minutes a pink solid precipitated, but dissolved again shortly after with the

Table 2
Refinement data for 1, 2, 3, 4, and 6. All data measured at 122(1) K.

	1	2	3	4	6
Molecular formula	$H_{86}C_{60}N_{12}O_{13}F_6Cl_5Li_2Cr_3$	$H_{30}C_{22}N_4O_{10}F_2Na_1Cr_1$	$C_{15}H_{16\cdot11}CrF_3N_3O_{2.56}$	$C_{198.84}H_{197.36}B_4Cr_6\ F_{18}N_{18}Na_4O_{13.61}$	$C_{78}H_{114}B_2N_9O_3F_9Na_2Cr_3$
Molecular weight	1644.585	623.485	388.32	3846.12	1620.38
Crystal system	Orthorhombic	Tetragonal	Monoclinic	Triclinic	Triclinic
Space group	$Pna2_1$	$P4/ncc$	$P21/c$	$P\bar{1}$	$P\bar{1}$
a (Å)	17.8140 (15)	12.5740(19)	10.2811(5)	16.126(3)	17.228(2)
b (Å)	9.036 (4)	12.5740(19)	9.7077(6)	17.1530(18)	17.417(2)
c (Å)	47.539 (5)	17.271(3)	16.1058(10)	20.433(2)	17.5370(18)
α (°)	90.00	90.00	90.00	104.670(9)	91.713(15)
β (°)	90.00	90.00	100.101(5)	103.809(8)	118.118(13)
γ (°)	90.00	90.00	90.00	112.454(10)	115.164(7)
V (Å^3)	7652 (3)	2730.6(6)	1582.54(15)	4684.1(12)	4022.0(8)
Z	12	4	4	1	2
F_{000}	3660	1292	794.0	1798	1708
D_{cal} (Mg m^{-3})	1.548	1.517	1.630	1.363	1.338
μ (mm^{-1})	0.72	0.51	0.777	0.419	0.482
Crystal size (mm)	0.34 × 0.31 × 0.24	0.46 × 0.23 × 0.20	0.282 × 0.074 × 0.059	0.177 × 0.165 × 0.104	0.068 × 0.079 × 0.155
Color	Pink	Pink	Violet	Light purple	Purple
θ range (°)	1.7–30.1	2.9–45.6	2.0–30.0	1.39–26.54	1.35–30.13
h	−25 → 25	−20 → 25	−14 → 14	−20 → 20	−24 → 24
k	−12 → 11	−25 → 25	−13 → 13	−21 → 21	−24 → 24
l	−66 → 66	−25 → 34	−22 → 22	−25 → 25	−24 → 24
Absorb. correction T_{min}, T_{max}	0.820, 0.886	0.858, 0.919	0.847, 0.961	0.916, 0.965	0.781, 0.942
No. measured reflections	69341	79590	47110	153838	104189
No. independent reflections	19719	5784	4600	19468	23630
No. reflections with $I > 2\sigma(I)$	14647	4307	3698	14813	15354
R_{int}	0.039	0.0639	0.0611	0.0683	0.0743
Number of ref. parameters	910	91	227	1205	1097
$R[F^2 > 2\sigma(F^2)]$	0.047	0.0330	0.0504	0.0708	0.0601
$wR(F^2)^{\dagger}$	0.116	0.0802	0.1251	0.1656	0.1277
S (Goodness of fit)	1.00	1.038	1.09	1.132	1.075
$\Delta\rho_{min}$, $\Delta\rho_{max}$(e Å^{-3})	−0.76, 0.97	−0.805, 1.047	−0.73, 0.94	−0.798, 1.904	−0.841, 1.525

continued warming. At a temperature of 50 °C the beaker was placed on ice and left for crystallization for ca. 1 h.

An intensely pink, crystalline product was isolated by filtration through a fritted filter funnel (porosity G3) and dryed by suction before placing it in a dessicator with conc. sulfuric acid. Yield: 10.886 g (81.5% of theoretical based on chromium). Analysis: calcd. for $C_{22}H_{30}N_4O_{10}F_2Na_1Cr_1$: H, 4.85%; C, 42.38%; N, 8.99%. Found: H, 4.58%; C, 42.39%; N, 8.90%.

MS (FAB + /m-NBA) *m/z* (relative intensity): 406.0 ($[Cr(py)_4F_2]^+$), 327.0 ($[Cr(py)_3F_2]^+$), 248.0 ($[Cr(py)_2F_2]^+$), 229.0 ($[Cr(py)_2F]^{2+}$).

Crystals suitable for X-ray were obtained by a modification of the above procedure: the reaction was performed at a smaller scale (ca. 1/50) and with further addition of water so that the reactants could be dissolved completely by heating to 65 °C on a water bath. Upon filtering and cooling, the reaction mixture was left for crystallization giving crystals of X-ray quality upon 2–3 h standing.

3.2.3. $[CrF_3(terpy)]\cdot 2.5H_2O$ (3)

Crude *mer*-$CrF_3(py)_3$ (0.870 g, 2.51 mmol) and 2,2′;6′,2″-terpyridine (0.600 g, 2.57 mmol) were suspended in 2-methoxyethanol (30 ml) and heated to reflux for 2 h. The solution was evaporated to 1/3 of the volume and cooled to RT. Water (0.5 ml) and acetone (30 ml) was added resulting in precipitation of a violet crystalline product. Yield 0.801 g (82%). The procedure yielded directly crystals suitable for X-ray diffraction. Analysis: calcd. for $C_{15}H_{16}N_3O_{2.5}F_3Cr$: H, 4.16%; C, 46.52%; N, 10.85%. Found: H, 4.09.%; C, 46.07; N, 10.81%.

3.2.4. $6[CrF_3(terpy)]\cdot 4Na(Bph_4)\cdot 6MeOH$ (4)

Solutions of $[CrF_3(terpy)]\cdot 2.5H_2O$ (40 mg, 0.10 mmol) in methanol (2 ml) and $Na(Bph_4)$ (40 mg, 0.11 mmol) in methanol (2 ml) were allowed to diffuse slowly together resulting in reddish crystals suitable for X-ray diffraction. Yield 44 mg (71%). The crystals loose methanol on standing. Analysis: calcd. for $C_{192}H_{170}B_4N_{18}O_6F_{18}Na_4Cr_6$: C, 63.80%; H, 4.74%; N, 6.97%. Found: C, 63.55%; H, 4.68%; N, 7.03%.

3.2.5. $[CrF_3(Me_3tacn)]\cdot 3.5H_2O$ (5)

Crude *mer*-$CrF_3(py)_3$ (1.00 g, 2.89 mmol) and Me_3tacn (0.55 g, 3.21 mmol) were dissolved in DMF (7 ml) and refluxed for 20 min. The resulting dark blue solution was cooled to 5 °C and filtered to yield 0.74 g (91%) of dark blue microcrystals which turn pinkish upon exposure to moisture. The crude product was dissolved in water (30 ml) whereto acetone (600 ml) was slowly added yielding 0.66 g of reddish needle shaped crystals. Analysis: calcd. for $C_9H_{28}N_3O_{3.5}F_3Cr$: H, 8.22%; C, 31.49%; N, 12.24%; Cr, 15.14%. Found: H, 8.24.%; C, 30.64; N, 11.89%; Cr, 16.45%. The discrepancies between elemental analyses and calculated composition of the X-ray structure reflects the varying degree of hydration of this compound, which can also be obtained in an anhydrous purple form.

3.2.6. $3[CrF_3(Me_3tacn)]\cdot 2Na(Bph_4)\cdot 2H_2O\cdot 2$-propanol (6)

Dilute solutions of $[CrF_3(Me_3tacn)]\cdot 3.5H_2O$ (12 mg, 0.035 mmol) in 2-propanol (5 ml) and $Na(Bph_4)$ (10 mg, 0.029 mmol) in 2-propanol (5 ml) were allowed to diffuse slowly together resulting in pink needle shaped crystals suitable for X-ray diffraction. Yield 15 mg (79%). Analysis: calcd. for $C_{78}H_{115}B_2N_9O_3F_9Na_2Cr_3$: C, 57.78%; H, 7.15%; N, 7.77%. Found: C, 58.02%; H, 7.13%; N, 7.68%.

3.3. Instruments and measurement

UV/vis spectra were recorded on a Perkin-Elmer, Lambda 2 UV/vis spectrophotometer. Elemental analysis for C, H and N was performed with a CE Instrument: FLASH 1112 series EA, at the microanalytic laboratory, University of Copenhagen. Elemental analysis for Cr and Na was done by AAS on a Perkin-Elmer 2280, and by flame emission on a Kipp H45 emission photometer, respectively. Fast-atom Bombardment Mass spectrometry (FAB+) was done on a Jeol JMS-HX 110 tandem mass spectrometer using *m*-nitrobenzyl alcohol as matrix. X-ray crystallographic data were collected on a Nonius KappaCCD diffractometer using graphite-monochromated Mo *Kα* radiation. Crystal structure and refinement data for 1, 2, 3, 4 and 6 are summarized in Table 2. For all five compounds, all non-hydrogen atoms were refined with anisotropic temperature factors. The molecular structure diagrams were made with the ORTEP-3 program [32].

3.4. DFT calculations

Calculations were performed with the Amsterdam Density Functional (ADF) program suite version 2003.02 or 2007.01 [33]. Slater-type orbital basis sets of triple-ζ quality for the valence orbitals were employed with polarization functions on the ligand atoms and additional valence p orbitals on Cr (ADF basis set TZ2P). Calculations were unrestricted, all-electron calculations with no frozen cores. Calculations were done using gradient corrected functionals employing the VWN LDA exchange-correlation functional supplemented with the non-local, Becke exchange [34] and Perdew correlation [35] functionals. No use of symmetry was made. All charge and spin densities were based on Mulliken analyses. Transition energies were evaluated by either Slater's transition state method [36] or the built-in TDDFT facilities of the program.

4. Conclusions

Several examples of minerals are known which contain fluoride complexes bridged by alkali metals *e.g.* $NaBF_4$ (ferruccite), Na_3AlF_6 (cryolite), K_2NaAlF_6 (elpasolite), Na_2LiAlF_6 (simmonsite). Here, it has been shown that similar structures can be targeted synthetically. Fluoride coordinated to chromium(III) interacts with protic solvents and small unpolarizable ions in solution as well as in the solid state. Efficient clustering of alkali metal cations by bridging uncharged complexes constitutes a new approach towards heterometallic systems. The pronounced tendency towards linear bridging by fluoride in these systems may render these interactions important in crystal engineering and in geometric control of polynuclear systems. Currently efforts along these lines are being undertaken. A strong effect on the auxiliary ligands by perturbation of coordinated fluoride ligands has been identified by DFT modeling. This result signals a warning regarding interpreting solvatochromism and spectral interaction with alkali metal cations in the framework of the traditional additive ligand-field models.

Supplementary data

Crystallographical data of *catena*-$[Na(H_2O)_4][Cr(py)_4F_2](HCO_3)_2$, *trans*-$[CrF_2(py)_4][Cr(py)_4F(\mu\text{-}F)Li(H_2O)_3][Cr(py)_4F(\mu\text{-}F)Li(H_2O)_4]Cl_5\cdot 6H_2O$, $[CrF_3(terpy)]\cdot 2.5H_2O$, $6[CrF_3(terpy)]\cdot 4Na(Bph_4)\cdot 6MeOH$, and $3[CrF_3(Me_3tacn)]\cdot 2Na(Bph_4)\cdot 2H_2O\cdot 2$-propanol, and have been deposited with the Cambridge Crystallographic Data Centre allocated with the deposit numbers CCDC 767058, CCDC 767059, CCDC 767060, CCDC 767062, and CCDC 767061, respectively. Copy of the data can be obtained free of charge on application to CCDC, 12 Union Road, Cambridge C2B 1EZ, UK, fax: +44 1223 336033, e-mail: deposit@ccdc.cam.ac.uk. Input and partial ADF output for geometry optimization on *fac*-$CrF_3(NH_3)_3$ as well as input for the Slater-TS calculation of the lowest quartet–quartet transition is available as supplementary information.

Acknowledgements

Prof. C.E. Schäffer and assoc. prof. J. Glerup are thanked for valuable discussions. The authors gratefully acknowledges financial support from the Danish Research Councils (JB, SP and HW grants).

Appendix A. Supplementary data

Supplementary data associated with this article can be found, in the online version, at doi:10.1016/j.jfluchem.2010.06.003.

References

[1] G.A. Jeffrey, An Introduction to Hydrogen Bonding, Oxford University Press, Oxford, UK, 1997.
[2] C.J.D. Craig, M.H. Brooker, J. Sol. Chem. 29 (2000) 879–888.
[3] J. Emsley, D.J. Jones, R.S. Osborn, J. Chem. Soc., Chem. Commun. 15 (1980) 703–704.
[4] L. Cheng, X. Xu, Y. Xu, Acta Crystallogr. E 64 (2008) m82.
[5] A.J. Norquist, C.L. Stern, K.R. Poeppelmeier, Inorg. Chem. 38 (1999) 3448–3449.
[6] N.N. Greenwood, A. Earnshaw, Chemistry of the Elements, 2nd ed., Butterworth & Heinemann, Amsterdam, 2006.
[7] M.R. Marvel, R.A.F. Pinlac, J. Lesage, C.L. Stern, K.R. Poeppelmeier, Z. Anorg. Allg. Chem. 635 (2009) 869–877.
[8] M.R. Marvel, J. Lesage, J. Baek, P.S. Halasyamani, C.L. Stern, K.R. Poeppelmeier, J. Am. Chem. Soc. 129 (2007) 13963–13969.
[9] R.Z. LeGeros, R. Kijkowska, W. Jia, J.P. LeGeros, J. Fluorine Chem. 41 (1988) 53–64.
[10] S. Kaizaki, H. Takemoto, Inorg. Chem. 29 (1990) 4960–4964.
[11] Y. Terasaki, S. Kaizaki, J. Chem. Soc., Dalton Trans. (1995) 2837–2841.
[12] Y. Terasaki, T. Fujihara, T. Schönherr, S. Kaizaki, Inorg. Chim. Acta 259 (1999) 84–90.
[13] R.J. Bianchini, U. Geiser, H. Place, S. Kaizaki, Y. Morita, J.I. Legg, Inorg. Chem. 25 (1986) 2129–2134.
[14] A. Bodner, P. Jeske, T. Weyhermuller, K. Wieghardt, E. Dubler, H. Schmalle, B. Nuber, Inorg. Chem. 31 (1992) 3737–3748.
[15] P. Yu, E.F. Murphy, H.W. Roesky, P. Lubini, H.-G. Schmidt, M. Noltemeyer, Organometallics 16 (1997) 313–316.
[16] B.F. Straub, F. Rominger, P. Hofmann, Inorg. Chem. 39 (2000) 2113–2119.
[17] L.F. Jones, C.A. Kilner, M.P. de Miranda, J. Wolowska, M.A. Halcrow, Angew. Chem., Int. Ed. 46 (2007) 4073–4076.
[18] D. Riou, F. Taulelle, G. Ferey, Inorg. Chem. 35 (1996) 6392–6395.
[19] D. Stalke, F.-Q. Liu, H.W. Roesky, Polyhedron 15 (1996) 2841–2843.
[20] T. Birk, J. Bendix, H. Weihe, Acta Crystallogr. E64 (2008) m369–m370.
[21] G. Fochi, J. Strahle, F. Gingl, Inorg. Chem. 30 (1991) 4669–4671.
[22] S.G. Thoma, F. Bonhomme, M. Nyman, M.A. Rodriguez, T.M. Nenoff, J. Fluorine Chem. 108 (2001) 73–77.
[23] N. Cloete, H.G. Visser, A. Roodt, Acta Crystallogr. E63 (2007) m45–m47.
[24] (a) K.R. Heier, J.A. Norquist, C.G. Wilson, C.L. Stern, K.R. Poeppelmeier, Inorg. Chem. 37 (1998) 76–80;
(b) P.C.R. Guillory, J.E. Kirsch, H.K. Izumi, C.L. Stern, K.R. Poeppelmeier, Cryst. Growth Des. 6 (2006) 382–389.
[25] (a) J. Bendix, A. Bøgevig, Inorg. Chem. 37 (1998) 5992–6001;
(b) J. Bendix, A. Bøgevig, Acta Crystallogr. C 54 (1998) 206–208.
[26] (a) C.C. Pye, T. Ziegler, Theor. Chem. Acc. 101 (1999) 396–408;
(b) A. Klamt, G. Schüürmann, J. Chem. Soc., Perkin Trans. 2 (1993) 799–805.
[27] (a) N. Buchholz, M. Leimkuhler, L. Kiriazis, R. Mattes, Inorg. Chem. 27 (1988) 2035–2039;
(b) L. Kiriazis, R. Mattes, Z. Anorg. Allg. Chem. 593 (1991) 90–98.
[28] F. Neese, J. Biol. Inorg. Chem. 11 (2006) 702–711.
[29] J. Glerup, J. Josephsen, E. Michelsen, E. Pedersen, C.E. Schäffer, Acta Chem. Scand. 24 (1970) 247–254.
[30] N. Costachescu, J. Chem. Soc. 102 (1912) 493–499.
[31] K. Wieghardt, P. Chaudhuri, B. Nuber, J. Weiss, Inorg. Chem. 21 (1982) 3086–3090.
[32] L.J. Farrugia, J. Appl. Crystallogr. 30 (1997) 565–566.
[33] (a) G. te Velde, E.J. Baerends, Comput. Phys. 99 (1992) 84–98;
(b) G. te Velde, F.M. Bickelhaupt, S.J.A. van Gisbergen, C.F. Guerra, E.J. Baerends, J.G. Snijders, T. Ziegler, J. Comp. Chem. 22 (2001) 931–967.
[34] A.D. Becke, Phys. Rev. A38 (1988) 3098–3100.
[35] (a) J.P. Perdew, Phys. Rev. B33 (1986) 8822–8824;
(b) J.P. Perdew, Phys. Rev. B34 (1987) 7406 (erratum).
[36] J.C. Slater, Quantum Theory of Molecules and Solids, McGraw-Hill, New York, 1974.